

Freeze-in leptogenesis with sterile neutrino self-interactions

María Dias Astros and Stefan Vogl

Institute of Physics, University of Freiburg,
Herrmann-Herder-Str. 3, 79104 Freiburg, Germany

E-mail: maria.dias@physik.uni-freiburg.de, stefan.vogl@physik.uni-freiburg.de

Abstract. Sterile neutrinos are a simple yet compelling addition to the Standard Model. For right-handed neutrinos with masses below the electroweak scale, leptogenesis can proceed through CP-violating oscillations of the sterile neutrinos. This is known as ARS or freeze-in leptogenesis. However, the ARS scenario requires the right-handed neutrinos to have a high degree of mass degeneracy. In this work, we study an extension of the SM that introduces a scalar singlet in addition to the two sterile neutrinos required to generate the baryon asymmetry. The new scalar interacts with the sterile neutrinos via a Yukawa interaction. This leads to an additional rate for the production and destruction of the sterile neutrinos and to a novel contribution to the effective potential. For the case in which the mass and the new Yukawa matrices are not diagonal in the same basis, we find that the effective potential can boost the baryon asymmetry of the universe by several orders of magnitude. This significantly alleviates the fine-tuned mass condition required in vanilla ARS leptogenesis.

Contents

1	Introduction	1
2	Basics of freeze-in leptogenesis	2
2.1	The ARS mechanism	2
2.2	The quantum kinetic equation	4
3	Sterile neutrino self-interactions	7
3.1	Numerical solutions	8
3.2	Analytic solution	11
4	Conclusions	15
A	The Casas-Ibarra parametrization	15
B	Analytical approach to standard ARS	16

1 Introduction

The Standard Model of particle physics (SM) is widely regarded as one of the most successful theories in modern physics. However, it is well-established that the SM fails in explaining various phenomena, including dark matter, dark energy, neutrino masses, and the baryon asymmetry of the universe. Thus, the SM remains an incomplete theory of nature. Sterile neutrinos, as one of the most minimal and compelling extensions of the SM, are promising candidates for addressing several of its key shortcomings. They have the potential to provide insights into the origin of neutrino masses, the nature of dark matter, and the baryon asymmetry of the universe (BAU). The latter refers to the Standard Model’s inability to account for the observed matter-antimatter imbalance that is quantified by the baryon-to-entropy ratio¹ [1–3]

$$\frac{B}{s} = \frac{n_b - n_{\bar{b}}}{s} \approx 8 \times 10^{-10},$$

where s is the entropy density of the universe and $n_{b,\bar{b}}$ are the number densities of baryons and antibaryons, respectively. Leaving aside the possibility that the BAU is the result of fine-tuned initial conditions, numerous ideas have been put forward to give a dynamical explanation for the observed value. Among these, leptogenesis [4], has become a very active field of research, particularly in the wake of the discovery of neutrino oscillations. In these scenarios, the BAU is produced in the leptonic sector and subsequently transferred to baryons via sphalerons [5]. Leptogenesis is specially compelling because it appears as a generic mechanism to generate the BAU in type I seesaw scenarios that also account for the lightness of the active neutrinos. In its original implementation, the SM is extended by the introduction of sterile neutrinos with masses well above the electroweak scale. These are responsible for generating the BAU through their out-of-equilibrium decays. This mechanism is known as thermal or freeze-out leptogenesis, as the right-handed neutrinos (RHNs) (produced during reheating)

¹It is also common to quantify the BAU by the baryon-to-photon ratio $\eta = (n_b - n_{\bar{b}})/n_\gamma \approx 6 \times 10^{-10}$ with n_γ the number density of photons.

are initially in thermal equilibrium with the SM plasma. Nonetheless, models of leptogenesis with lighter sterile neutrinos, potentially accessible in current and future experiments, are very intriguing. These include, e.g. the neutrino minimal SM (ν MSM) [6–10] and resonant leptogenesis [11, 12]. The ν MSM, in particular, makes use of an idea proposed by Akhmedov, Rubakov and Smirnov (ARS) where sterile neutrinos with masses of a few GeV can generate the BAU through their CP-violating oscillations [13]. In this scenario, total lepton number is approximately conserved at high temperatures, but it is redistributed among the active and sterile sectors. Lepton number in the active sector is then partially converted into a baryon asymmetry via sphaleron transitions. In this case, one assumes that no RHNs were present right after inflation and the small Yukawa couplings connecting the active and sterile sectors guarantee that at least one of the sterile states remains out-of-equilibrium until sphaleron freeze-out. ARS is therefore a *freeze-in scenario*.

However, one of the main drawbacks of the vanilla ARS is that it requires significant mass degeneracy among the sterile neutrinos to achieve the observed BAU. In particular, for the case of two RHNs with masses between 1 GeV and 10 GeV, successful leptogenesis requires a mass splitting of $|M_1 - M_2| \lesssim 10^{-5}$ GeV [14]. Moreover, although lighter sterile neutrinos are kinematically accessible in many current experiments, this advantage is counterbalanced by the tiny Yukawa couplings $\sim \mathcal{O}(10^{-7})$ which are very challenging to probe [15]. To resolve this issue, and further motivated by the potential occurrence of additional fields in nature, some attention has been given to models featuring interactions among the sterile neutrinos (see e.g. [16, 17]). Certainly, new interactions in the sterile sector could improve future detection prospects. Yet, it has been shown that including interactions that could bring the RHNs into equilibrium earlier can lead to a reduction in the generated BAU and, in best-case scenarios, only to an $\mathcal{O}(1)$ enhancement with respect to the vanilla ARS [16, 17]. Other extensions of the minimal sterile neutrino framework and their impact on ARS leptogenesis were studied, e.g. in [18–20].

In this work, we focus on the first issue, namely the mass degeneracy in the vanilla ARS. The goal of this work is to investigate if self-interactions among the sterile neutrinos can relax the mass degeneracy required in vanilla ARS. For this purpose we study a setup with two sterile neutrinos interacting via a scalar singlet. This is similar to the model considered in [16, 17] but we allow for a more general structure of Yukawa couplings than these previous works.

This paper is structured as follows. Section 2 provides a brief introduction to the ARS mechanism, outlining how the asymmetry is generated in the vanilla scenario, and we present the quantum kinetic equation (QKE) governing the evolution of the BAU. In Section 3, we explore the inclusion of the effects of neutrino self-interactions in the equations and present the corresponding numerical results. To put this in perspective we derive an approximate analytical solution in the oscillatory regime and highlight the key differences between the vanilla ARS and the extended model. Finally, Section 4 offers our conclusions and provides an outlook for future work.

2 Basics of freeze-in leptogenesis

2.1 The ARS mechanism

We begin by giving a brief review of the ARS mechanism [13] and summarizing how the baryon asymmetry is generated within this scenario (for a more complete discussion see e.g. the review [14]). The Lagrangian of the model corresponds to a type I seesaw mechanism. In

its minimal incarnation, the SM is extended by two right-handed neutrinos². The Lagrangian thus reads

$$\mathcal{L} = \mathcal{L}_{\text{SM}} + i\bar{N}_i \not{\partial} N_i - \frac{1}{2} \bar{N}_i M_{ij} N_j - \left(F_{ai}^\dagger \bar{L}_a \epsilon \Phi N_i + h.c. \right), \quad (2.1)$$

where \mathcal{L}_{SM} is the Lagrangian of the SM, N_i are the RH neutrinos and Φ and $L = (\nu_L, e_L)^T$ are the SM Higgs and left-handed lepton doublets, respectively. Here, M is the Majorana mass matrix of the RH neutrinos, F are the Yukawa matrices connecting the sterile sector with the SM and ϵ is the 2×2 antisymmetric tensor, i.e. $\epsilon^{12} = -\epsilon^{21} = 1$. From now on we will work in the mass basis, i.e. the basis in which M is diagonal.

As pointed out by Sakharov in the 70's, a mechanism capable of generating the baryon asymmetry must fulfill three conditions [21]: i) baryon number violation, ii) C and CP violation and iii) deviation from equilibrium. In the SM baryon number and C-symmetry are violated by the weak sphalerons and the weak interactions, respectively. However, CP violation is small in the SM and, in addition, a significant departure from thermal equilibrium is not expected. The first of these shortcomings is naturally addressed by the seesaw mechanism since it provides additional sources of CP violation in the mixing in the neutrino sector, i.e. encoded in complex phases present in the Yukawa coupling matrix F . Moreover, new processes involving the sterile neutrinos open up the possibility of departure from thermal equilibrium. For instance, in its original proposal, thermal leptogenesis relies on the out-of-equilibrium decay of the heavy RHNs, whereas in the ARS mechanism non-equilibrium is established due to the tiny couplings of light steriles which are produced from the SM through freeze-in.

The creation of the baryon asymmetry in the ARS model unfolds via the interplay of multiple interlocking processes. In the oscillatory regime, these neatly separate into three stages that are controlled by different timescales. For convenience, let us define a dimensionless time variable $z = T_{\text{ws}}/T$, where T_{ws} is a reference temperature that is taken to be $T_{\text{ws}} \simeq 130$ GeV, i.e. the temperature at which sphalerons freeze-out. In the first stage, right-handed neutrinos are produced at very high temperatures in flavour states. Since F and M are not diagonal in the same basis, they start oscillating at a scale z_{osc} given by

$$z_{\text{osc}} = T_{\text{ws}} \left(\frac{216 \zeta(3)}{a_R \pi |\Delta M^2|} \right)^{1/3}, \quad (2.2)$$

with the squared mass difference defined as $|\Delta M^2| = |M_1^2 - M_2^2|$. Here $a_R = m_{Pl} \sqrt{\frac{45}{4\pi^3 g_*}}$ with $m_{Pl} = 1.22 \times 10^{19}$ GeV being the Planck mass and $g_* = 106.75$ denoting the effective number of relativistic degrees of freedom. These CP-violating oscillations lead to the generation of flavour asymmetries in the active sector

$$L_a(z > 0) = \frac{n_a - n_{\bar{a}}}{s} \neq 0, \quad a = e, \mu, \tau, \quad (2.3)$$

with s the entropy density of the universe and $n_{a(\bar{a})}$ the number densities of the active (anti) leptons.

²Even though in the original ARS mechanism the SM is extended with three sterile neutrinos, only two are enough to generate a baryon asymmetry. For the sake of simplicity we, therefore, consider this minimal case.

However, since there is no total lepton number violating processes³, total lepton number remains zero throughout, namely

$$L_{\text{tot}} = \sum_{i=1,2} q_{N_i} + 2 \sum_{a=e,\mu,\tau} L_a = 0. \quad (2.4)$$

Here the factor of two accounts for the SU(2) multiplicity of the active doublets and the sterile charges are analogously defined as

$$q_{N_i} = \frac{n_i^+ - n_i^-}{s}, \quad i = 1, 2, \quad (2.5)$$

where we denote the "plus" and "minus" helicities, which play the role of particle and antiparticles in the sterile sector. Note that, through the Yukawa couplings, lepton number is redistributed between the sterile and active sectors.

In the final step, as long as the temperature remains above T_{ew} (for $z \lesssim 1$), a portion of the active lepton asymmetries L_a is reprocessed by weak sphalerons, resulting in a net baryon number. It is interesting to note, that for $z \ll z_{\text{osc}}$ the oscillation phase is still very small and the generation of the flavour asymmetries is suppressed [16]. On the other hand, for $z \gg z_{\text{osc}}$ the oscillations become very rapid and the contributions to the asymmetry average to zero. The bulk of the asymmetry is therefore produced around $z \sim z_{\text{osc}}$, corresponding to the time when the sterile neutrinos undergo the first oscillations. Another crucial time scale in the system is the point at which the abundance of right-handed neutrinos reaches thermal equilibrium, at $z_{\text{eq}} \propto (|F^* F^T|)^{-1}$, with $|\cdot|$ denoting the absolute value of the largest eigenvalue. Importantly, at least one neutrino species must remain out of equilibrium until after $z = 1$, as the third Sakharov condition would be violated otherwise.

If the Yukawa couplings are sufficiently small one can get an analytical estimation for the resulting asymmetry by using a perturbative calculation in F [6, 22, 23] which leads to

$$\frac{B}{s} \propto |F^* F^T|^3 \left(\frac{\Delta M^2}{\text{GeV}^2} \right)^{-2/3}. \quad (2.6)$$

This result is well-known and it is one of the main drawbacks for the ARS mechanism. Plugging in numbers for the Yukawa couplings F , one finds that, one can obtain the observed value of the BAU only for very degenerate neutrino masses $M_i M_j \gg |\Delta M^2| \sim 10^{-5} \text{GeV}^2$ ⁴.

2.2 The quantum kinetic equation

In the most general case, the dynamics of the system is governed by the kinetic equation for the complete neutrino density matrix ρ . It reads [25–27]

$$i \frac{d\rho}{dt} = [\mathbb{H}, \rho] - \frac{i}{2} \{ \Gamma, \rho \} + \frac{i}{2} \{ \Gamma^p, \mathbb{I} - \rho \}, \quad (2.7)$$

where $\mathbb{H}(k) = H^0(k) + V(k)$ is the effective Hamiltonian, consisting of the free Hamiltonian $[H^0(k)]_{ij} = (k^2 + M_I^2)^{1/2} \delta_{ij}$ and the effective potential $V(k)$ which is induced by medium effects. Here, k represents the momentum of the neutrinos, M_I their corresponding masses,

³This holds for $z < 1$ if the Majorana masses for the sterile neutrinos are very small given that total lepton number violation is a M^2/T effect [22].

⁴See [24] for a case of freeze-in leptogenesis with non-degenerate spectra.

while Γ and Γ^p are the destruction and production rates, respectively. Following Refs. [6, 28] we can approximate the last term in (2.7) simply as Γ^p assuming Boltzmann statistics, i.e. $\mathbb{I} - \rho \approx \mathbb{I}$. Moreover, since the equilibrium density matrix $\rho_{\text{eq}} = \exp(-\mathbb{H}/T) \approx \exp(-k/T)$ must satisfy (2.7) one can rewrite the production rate as $\Gamma^p = \frac{1}{2} \{\Gamma, \rho_{\text{eq}}\}$. Formally, ρ is a 10×10 matrix, where the diagonal elements correspond to occupation numbers whereas the off-diagonal elements describe flavour correlations. By performing a series of simplifications (see e.g. [6]) ρ is reduced to a block-diagonal matrix, consisting of two 3×3 matrices describing the active (anti-)neutrino system and two 2×2 non-diagonal matrices representing the sterile sector. Since the oscillations of the active neutrinos do not play a role on the scales considered here, their sub-matrices can be reduced to the diagonal elements corresponding to the occupation numbers. The sterile neutrinos, on the other hand, need to be treated using a full quantum approach, such that all the elements of their density matrix remain relevant. It follows that the dynamics of the system will be determined by the evolution of the eigenvalues of \mathbb{H} and Γ . In fact, it is precisely the misalignment between \mathbb{H} and Γ , which in general are not diagonal in the same basis, that leads to the oscillations in the sterile sector. After the simplifications, one is left with two 2×2 density matrices for the sterile neutrinos and six active (anti-)neutrino occupation numbers.

For simplicity, from now on, we will work with an integrated version of Eq. (2.7) that allows us to remove the momentum dependence from both sides of the evolution equation. With this in mind we start by parametrizing the density matrix for the sterile neutrinos as

$$\rho_{N^\pm}(k) = \rho_{\text{eq}}(k) + \delta\rho_{N^\pm}, \quad (2.8)$$

where we indicate the "plus" and "minus" helicities and $\delta\rho$ denotes the deviation from equilibrium which we assume is independent of momenta. Here and in the following we adopt the notation of [23] and use their expressions. Further one can take the thermal average of all the operators, i.e.

$$\langle \mathcal{O} \rangle = \frac{\int dk k^2 \mathcal{O} \rho_{\text{eq}}}{\int dk k^2 \rho_{\text{eq}}}, \quad (2.9)$$

with ρ_{eq} the equilibrium distribution. Additionally, it is convenient to rewrite Eq. (2.7) in terms of the dimensionless quantity z . To this end, we use the time derivative in an expanding universe given by

$$\frac{d}{dt} = \frac{\partial}{\partial t} - Hk \frac{\partial}{\partial k}, \quad (2.10)$$

where $H = \frac{T^2}{a_R}$ is the Hubble expansion rate for a radiation dominated universe. By incorporating all these simplifications, we obtain an equation describing the evolution of the deviations of the heavy neutrinos' number density from equilibrium. Defining δn in analogy with $\delta\rho$ one finds [23]

$$\frac{d\delta n_{N^\pm}}{dz} = -\frac{i}{2} [H_{N^\pm}^{\text{th}} + z^2 H_{N^\pm}^{\text{vac}}, \delta n_{N^\pm}] - \frac{1}{2} \{\Gamma_{N^\pm}, \delta n_{N^\pm}\} + \sum_{a,b=e,\mu,\tau} \tilde{\Gamma}_{N^\pm}^a (A_{ab} + C_b/2) \Delta_b. \quad (2.11)$$

Here, the first term on the right-hand side contains the contributions from the Hamiltonian, the second term accounts for the contributions from the rate, and the third term corresponds to the SM back reaction. The effective Hamiltonian in vacuum $H_{N^\pm}^{\text{vac}}$ and the corresponding

finite temperature corrections $H_{N^\pm}^{\text{th}}$ are given by

$$\begin{aligned} H_{N^\pm}^{\text{vac}} &= \frac{\pi^2}{18\zeta(3)} \frac{a_R}{T_{\text{ws}}^3} \left(\text{Re}[M^\dagger M] \pm i\text{Im}[M^\dagger M] \right), \\ H_{N^\pm}^{\text{th}} &= h_{\text{th}} \frac{a_R}{T_{\text{ws}}} \left(\text{Re}[F^* F^T] \mp i\text{Im}[F^* F^T] \right), \end{aligned} \quad (2.12)$$

with $h_{\text{th}} \approx 0.23$. Meanwhile, the rates appearing in the collision terms of Eq. (2.11) are defined as follows

$$\begin{aligned} \Gamma_{N^\pm} &= \gamma_{AV} \frac{a_R}{T_{\text{ws}}} \left(\text{Re}[F^* F^T] \mp i\text{Im}[F^* F^T] \right), \\ \left(\tilde{\Gamma}_{N^\pm}^a \right)_{ij} &= \pm \frac{1}{2} \gamma_{AV} \frac{a_R}{T_{\text{ws}}} \left(\text{Re}[F_{ia}^* F_{aj}^T] \mp \text{Im}[F_{ia}^* F_{aj}^T] \right), \end{aligned} \quad (2.13)$$

where $\gamma_{AV} = 0.012$. The coefficients on the last term of Eq. (2.11) are given by

$$A = \frac{1}{711} \begin{pmatrix} -221 & 16 & 16 \\ 16 & -221 & 16 \\ 16 & 16 & -221 \end{pmatrix}, \quad C = -\frac{8}{79} (1 \ 1 \ 1). \quad (2.14)$$

On the other hand, the evolution of the SM-conserved charges $\Delta_a = B/3 - L_a$ is described by the equation

$$\frac{d\Delta_a}{dz} = \frac{\gamma_{AV}}{2} \frac{a_R}{T_{\text{ws}}} \sum_i F_{ia} F_{ai}^\dagger \left(\sum_b (A_{ab} + C_b/2) \Delta_b - q_{N_i} \right) - \frac{S_a}{T_{\text{ws}}}, \quad (2.15)$$

with the source term

$$S_a = \gamma_{AV} a_R \sum_{\substack{i,j \\ i \neq j}} F_{ia}^* F_{ja} \left\{ i\text{Im}[(\delta n_N)_{ij}^{\text{even}}] + \text{Re}[(\delta n_N)_{ij}^{\text{odd}}] \right\}. \quad (2.16)$$

Here we have defined the even and odd contributions as

$$\delta n_N^{\text{even}} = \frac{\delta n_{N^+} + \delta n_{N^-}}{2} \quad \text{and} \quad \delta n_N^{\text{odd}} = \frac{\delta n_{N^+} - \delta n_{N^-}}{2}, \quad (2.17)$$

so that the sterile charges are given by $q_{N_i} = 2(\delta n_N)_{ii}^{\text{odd}}$. It is important to note that Eq. (2.11) is valid only for relativistic neutrinos, as we neglect their mass in all terms except for $H_{N^\pm}^{\text{vac}}$. This approximation is reasonable provided that the masses of the heavy neutrinos are of the order of a few GeV. The net baryon asymmetry is frozen-in at the time of sphaleron freeze-out and is given by

$$B = \frac{28}{79} [\Delta_1(z) + \Delta_2(z) + \Delta_3(z)]|_{z=1}. \quad (2.18)$$

A detailed review of the analytical solution of Eqs. (2.11) and (2.15) using a perturbative expansion in F [23] is provided in Appendix B.

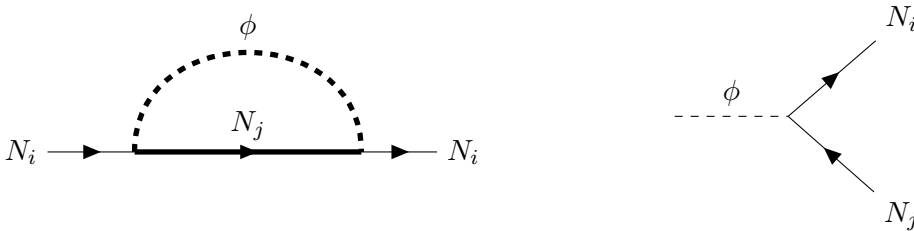


Figure 1: Leading order contributions from the new interaction of RH neutrinos in freeze-in leptogenesis.

3 Sterile neutrino self-interactions

In this section we explore how the picture changes when we allow for self-interactions among the sterile neutrinos. Specifically, we will consider interactions of the neutrinos with a scalar singlet ϕ . For simplicity, we assume ϕ to be in thermal equilibrium with the SM plasma. The interaction Lagrangian for the scalar-sterile neutrino coupling is given by

$$\mathcal{L}_{\text{int}} = Y_{ij} \bar{N}_i N_j \phi, \quad (3.1)$$

where Y is a 2×2 real and symmetric matrix. This new term would lead to the generation of masses for the sterile neutrinos if ϕ acquires a vacuum expectation value. If this is the only contribution to the mass, Y is diagonal in the same basis as the mass matrix M . However, in our discussion, we do not assume a specific origin for the heavy neutrino masses, allowing for the more general case where Y and M are independent. This is the key difference between this study and previous works of ARS leptogenesis in scalar extensions where, either a diagonal Yukawa matrix was assumed [16] or the neutrino masses were generated by ϕ directly [17]. As we will see later, the fact that we allow M and Y to be diagonal in different bases leads to an enhancement of the produced BAU through thermal effects in the dispersion relation of the sterile neutrinos.

The interaction term modifies Eq. (2.7) in two ways. First, forward scattering of sterile neutrinos in the hot plasma alters their dispersion relation, appearing as a new contribution to the thermal potential [29, 30], i.e. $\mathbb{H} = H^0 + H_{\text{SM}}^{\text{th}} + H_{\phi}^{\text{th}}$. The lowest order corrections appear at one loop level in the bubble diagram shown in the left panel of Fig. 1. Assuming the scalar to be sufficiently light ($m_{\phi} \ll T$), the thermal potential takes the form

$$H_{\phi}^{\text{th}}(k) = Y \cdot Y^T \frac{T^2}{24k} \rightarrow \langle H_{\phi}^{\text{th}} \rangle = Y \cdot Y^T \frac{T\pi^2}{432\zeta(3)}, \quad (3.2)$$

where we have taken the thermal average as in Eq. (2.9), see e.g. [31] for more details on the computation of the potential. Second, the new interaction introduces additional production and destruction channels for the sterile neutrinos via the decay and inverse decay of the scalar (see right panel of Fig. 1). For the decay of the scalar $\phi \rightarrow \bar{N}_i N_j$ the thermally averaged rate is given by

$$\langle \Gamma_{\phi}^p \rangle \approx Y \cdot Y^T \frac{m_{\phi}^2 T^2}{72\pi n_{\phi}^{\text{eq}}}, \quad (3.3)$$

Parameters	
$m_2^2 = 7.41 \times 10^{-5} \text{ eV}^2$	$M_1 \approx M_2 = 1 \text{ GeV}$
$m_3^2 = 2.511 \times 10^{-3} \text{ eV}^2$	$\delta = \frac{3\pi}{2}$
$\sin^2(\theta_{12}) = 0.307$	$\alpha_1 = 0$
$\sin^2(\theta_{13}) = 0.02203$	$\alpha_2 = -2\pi$
$\sin^2(\theta_{23}) = 0.572$	$\omega = \frac{3\pi}{4} + 2.16i$

Table 1: The parameters used for the Casas-Ibarra parametrization of F .

where n_ϕ^{eq} is the equilibrium number density of the scalar. With these two new contributions Eq. (2.7) takes the following form

$$i \frac{d\rho}{dt} = \mathbb{C}_{\text{ARS}} + [H_\phi^{\text{th}}, \rho] - \frac{i}{2} \{ \Gamma_\phi^d, \rho^2 \} + \frac{i}{2} \Gamma_\phi^p, \quad (3.4)$$

where for the sake of readability we denote as \mathbb{C}_{ARS} the contribution from the ARS mechanism described in the previous section. Note that for the destruction rate associated with the new interaction, the anticommutator with ρ^2 is used, as the inverse decay of the scalar involves the annihilation of two sterile neutrinos. The destruction rate is connected to the production rate through the relation

$$\Gamma_\phi^d = \frac{\Gamma_\phi^p}{\rho_{\text{eq}}^2}. \quad (3.5)$$

As we will see, the new physics back reaction rate is not relevant in the parameter space we discuss in the following sections. The integrated version of Eq. (3.4) is

$$\begin{aligned} \frac{d\delta n_{N^\pm}}{dz} = & -\frac{i}{2} [H_{N^\pm}^{\text{th}} + z^2 H_{N^\pm}^{\text{vac}}, \delta n_{N^\pm}] - \frac{1}{2} \{ \Gamma_{N^\pm}, \delta n_{N^\pm} \} + \sum_{a,b=e,\mu,\tau} \tilde{\Gamma}_{N^\pm}^a (A_{ab} + C_b/2) \Delta_b \\ & - \frac{i}{2} [V_N, \delta n_{N^\pm}] - \frac{z^2}{n_{\text{eq}}} \{ \Gamma_\phi, \delta n_{N^\pm} \} - \frac{z^2}{2n_{\text{eq}}^2} \{ \Gamma_\phi, \delta n_{N^\pm}^2 \}, \end{aligned} \quad (3.6)$$

where, for simplicity, we have written all the contributions from the new interactions in the second line and the additional terms are given by

$$V_N = \frac{\pi^2 a_R}{432 \zeta(3) T_{\text{ws}}} Y \cdot Y^T, \quad \Gamma_\phi = \frac{\pi m_\phi^2 a_R n_\phi^{\text{eq}}}{72 \zeta(3) T_{\text{ws}}^3} Y \cdot Y^T. \quad (3.7)$$

3.1 Numerical solutions

In this section we will investigate the numerical solutions to Eq. (3.6). We will restrict ourselves to the oscillatory regime allowing us to make the connection to the discussion in Appendix B. Therefore we choose a rather small Yukawa coupling F that we keep fixed for the rest of this work. For this we use the Casas-Ibarra parametrization [32] (see Appendix A) with the parameters specified in Tab. 1. The parameters in the left column of the table, are taken from global analyses of different neutrino oscillation experiments [33] assuming the lightest of the active neutrinos to be massless and a normal mass ordering. The parameters in the right column cannot be directly constrained by oscillation experiments and we take the benchmark values used in [23] for convenience. In addition, for simplicity, we will consider the special case $Y_{ii} = Y_{jj}$. We fix the mass of the scalar to $m_\phi = 3 \text{ GeV}$ throughout.

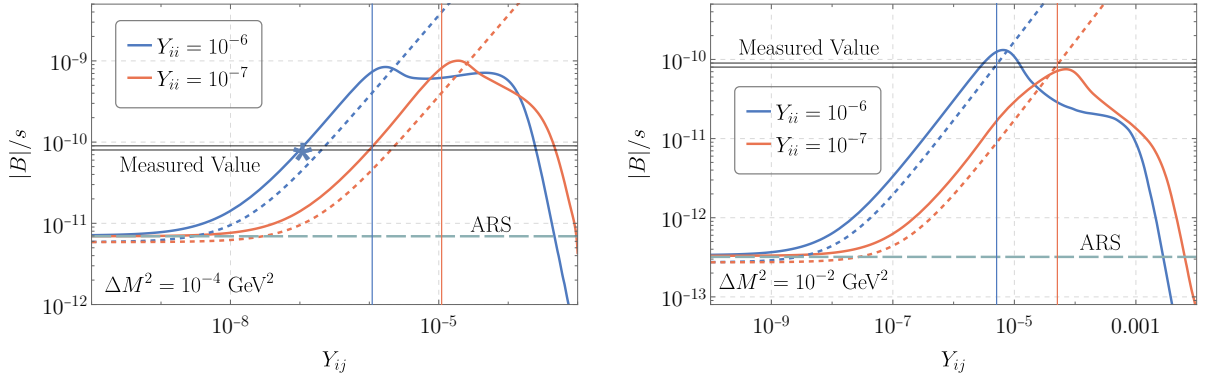


Figure 2: The baryon asymmetry with respect to the off-diagonal Yukawa components for a fixed value of the mass of the mediator $m_\phi = 3$ GeV and two different values for the diagonal components $Y_{ii} = 10^{-6}$ (solid blue) and $Y_{ii} = 10^{-7}$ (solid orange) and two different mass splittings $\Delta M^2 = 10^{-4}$ (left) and $\Delta M^2 = 10^{-2}$ (right). In light blue we indicate the value of the asymmetry obtained with the vanilla ARS for the corresponding mass splittings and in black the measured BAU. For completeness, as dashed lines we also show the analytical approximation (see Sec. 3.2 for more details) and the values of the Yukawa for which we expect it to break down. The blue star (left) indicates the benchmark discussed in the text.

Benchmark point				
ΔM^2	Y_{ii}	Y_{ij}	m_ϕ	$ B /s$
10^{-4} GeV ²	10^{-6}	1.1×10^{-7}	3 GeV	8.76×10^{-11}

Table 2: Parameters corresponding to the benchmark point discussed in the main text.

In Figure 2 we show the evolution of the asymmetry as a function of the off-diagonal components of the Yukawa coupling Y_{ij} for two fixed values of $Y_{ii} = 10^{-6}$ (blue) and $Y_{ii} = 10^{-7}$ (orange). The left panel corresponds to a mass splitting of $\Delta M^2 = 10^{-4}$ GeV² while the right panel corresponds to $\Delta M^2 = 10^{-2}$ GeV². For comparison, we also indicate with a dashed light blue line the value of the BAU that is generated in the vanilla ARS scenario for each mass splitting. The two solid black lines denote the range in which the measured value of the BAU lies, i.e. between 8×10^{-11} and 9×10^{-11} . In addition, the dashed blue and orange lines correspond to the analytical solutions discussed in detail in Sec. 3.2, while the vertical solid lines mark the values of the off-diagonal Yukawa couplings where the analytical approximations are expected to break down. We see that by the inclusion of the new interactions the generated BAU is enhanced by over two orders of magnitude. As a result, the measured value of the BAU can be achieved for square mass splittings significantly larger than those in the vanilla ARS case. As we will discuss in detail in the next section, the increase in the BAU observed to the left of the vertical lines is primarily driven by the effects of the sterile thermal potential. However, when the thermal potential becomes too large compared to $H_{N^\pm}^{\text{vac}}$ the asymmetry ceases to grow and begins to decline. The reason for this is essentially the same behind the suppression of the asymmetry by $(\Delta M^2)^{-2/3}$ in the vanilla ARS. In that case, a larger mass splitting results in a smaller typical oscillation scale z_{osc} , i.e. oscillations start

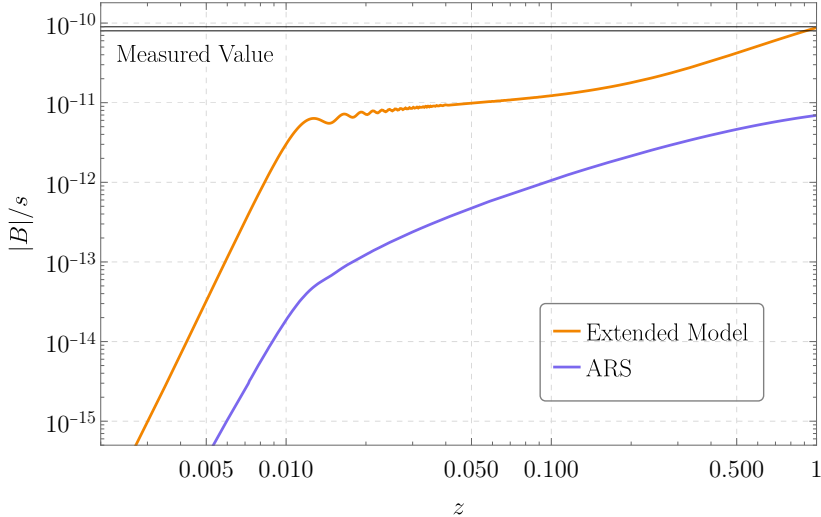


Figure 3: The evolution of the baryon asymmetry with respect to z for the benchmark point considered in this section (solid orange) and the vanilla ARS (solid purple) for comparison. The black horizontal lines denote the measured value of B .

at earlier times and there is a smaller population of sterile neutrinos at that moment which leads to a suppression. This is also true in a system where the oscillations are dominated by the squared thermal mass difference. In analogy to the vacuum mass, the thermal mass is defined as the eigenvalues of the thermal potential V_N such that the thermal mass difference is

$$\Delta M_{\text{thermal}} = \frac{4 \pi^2 a_R}{432 \zeta(3) T_{\text{ws}}} Y_{ii} Y_{ij}. \quad (3.8)$$

In a similar way, in the limit $\Delta M^2 \rightarrow 0$ the asymmetry is suppressed by $\Delta M_{\text{thermal}}^{-1}$. In the regime to the right of the solid vertical lines, the interplay between the two different oscillation scales makes the problem non-trivial and the suppression of the asymmetry by the thermal potential follows a different scaling. Increasing the coupling further, we note a subtle rise in the generated asymmetry. We assume that is due to the rate of decay of the scalar into two RHNs becoming effective but we do not have an analytic result that covers this regime. In any case, this behavior is transitional. At even larger coupling, the rate equilibrates the sterile neutrinos more efficiently than the SM one such that equilibrium is reached before sphaleron freeze-out. This leads to the strong suppression of the BAU that is apparent to the right side of Fig. 2. This decrease is in agreement with the results of [16, 17] whereas the increase, that depends on Y_{ij} , has been missed by them.

In Figure 3 we present the evolution of the BAU as a function of z for the benchmark point marked by a star in the left panel of Fig. 2. For this set of parameters, we find an asymmetry consistent with the measured value (see Tab. 2). For comparison, we also include the evolution of the BAU in the vanilla ARS, shown as a solid purple line. With the same mass splitting, the vanilla ARS produces a BAU that falls short by at least one order of magnitude at the time of sphaleron freeze-out. Additionally, we observe that the asymmetry deviates from the vanilla scenario from very early times, with noticeable wiggles appearing around $z = 0.01$. As we will discuss in the next section, these wiggles correspond to oscillations in the sterile charges.

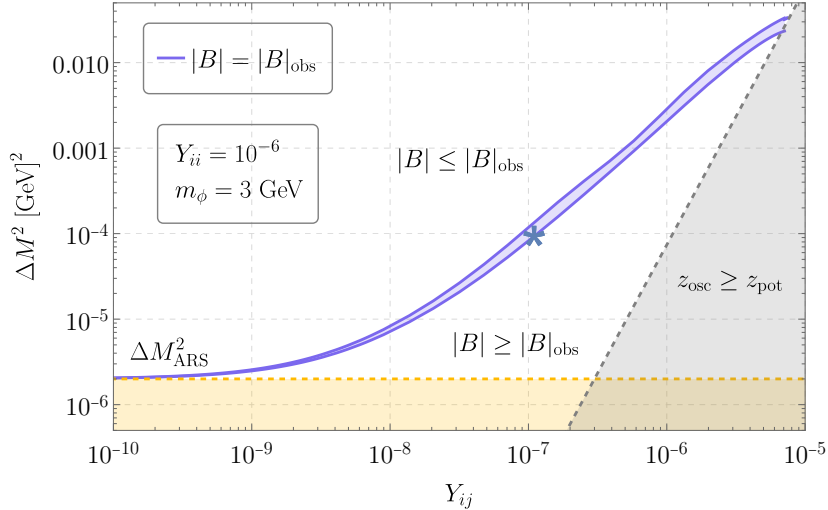


Figure 4: The parameter space in the $Y_{ij} - \Delta M^2$ plane for fixed values of $Y_{ii} = 10^{-6}$ and $m_\phi = 3 \text{ GeV}$. Everywhere between the purple lines the measured value of the BAU can be obtained. Above the upper purple line, the BAU is too small, while below the lower purple line, the BAU exceeds the observed limits. The dashed yellow line represents the mass splitting required in the vanilla ARS mechanism to achieve B_{obs} while the gray region indicates the region where our analytical approximation breaks down. For completeness we also indicate the benchmark point shown in the previous figure with a blue star.

Finally, figure 4 shows the parameter space in the $Y_{ij} - \Delta M^2$ plane for a fixed value of $Y_{ii} = 10^{-6}$. The region between the purple lines can account for the BAU within the observational error. Above the upper line the generated asymmetry is too small, while below the bottom line the BAU exceeds the observational limits. The dashed yellow line indicates the mass splitting required in the vanilla ARS scenario in order to generate B_{obs} . The gray area shows the region for which we expect our analytical approximation to break down.

3.2 Analytic solution

In this section we discuss an analytical solution for the scalar extension of the ARS mechanism. For convenience, the solution and its derivation for the standard ARS case are summarized in Appendix B. To simplify the problem, we assume $Y_{ii} = Y_{jj}$. As noted in section 2, the vanilla scenario involves two key time scales: z_{osc} , corresponding to the sterile oscillation phase during which most of the asymmetry is produced, and z_{eq} , associated with the equilibration of the neutrinos, which results in the washout of the asymmetry. In this work, we focus on scenarios where there is a distinct separation between the relevant scales, allowing the two processes to be treated independently. In particular, we will focus on the so-called oscillatory regime characterized by $z_{\text{osc}} \ll z_{\text{eq}}$, which occurs, for instance, when the Yukawa couplings are small. In the vanilla ARS scenario, the interplay between these two time scales will determine the evolution of the system.

This remains true for the scalar extension explored in this work. However, now two additional time scales come into play: one associated with the sterile thermal potential z_{pot}

and another linked to the new rate z_{decay} . These are given by

$$z_{\text{pot}} = \frac{216\zeta(3)T_{\text{ws}}}{\pi a_R Y_{ii} Y_{ij}} \quad \text{and} \quad z_{\text{decay}} = \left(\frac{18\zeta(3)T_{\text{ws}}^3}{\pi m_\phi^2 a_R Y_{ii} Y_{ij}} \right)^{1/3}, \quad (3.9)$$

where z_{pot} is defined in a manner analogous to z_{osc} , representing approximately the time when the sterile neutrinos undergo a full oscillation driven by the thermal mass difference. Similarly, z_{decay} denotes the time scale for the decay rate of the scalar to equilibrate. For the rate and the potential to play a significant role in the problem, we require $z_{\text{pot, decay}} \leq 1$. Under this condition, we find that the effects of the potential become relevant for $Y_{ij} \cdot Y_{ii} \gtrsim 10^{-14}$, while the rate only becomes important for $Y_{ij} \cdot Y_{ii} \gtrsim 2 \times 10^{-12}$ if we take $m_\phi = 3$ GeV. This allows us to neglect the effects of the rate since they appear at higher couplings and the thermal potential effectively dominates the evolution of the system in the parameter space of interest here. We then proceed in a similar way to App. B, performing a perturbative expansion in F . For $z \ll z_{\text{eq}}$, and neglecting the terms associated with the new rate, we can replace $(\delta n_{N^\pm})_{ij} \rightarrow -n_{\text{eq}} \delta_{ij}$ on the right-hand side of Eq. (3.6) which leads to

$$\frac{d}{dz} \delta n_{N_{ij}}^{\text{odd}} + i\Omega_{ij} z^2 \delta n_{N_{ij}}^{\text{odd}} = \frac{i}{2} V_{N_{ij}} \left(\delta n_{N_{ii}}^{\text{odd}} - \delta n_{N_{jj}}^{\text{odd}} \right) - i \text{Im}[F^* F^T]_{ij} G, \quad (3.10a)$$

$$\frac{d}{dz} \delta n_{N_{ij}}^{\text{even}} + i\Omega_{ij} z^2 \delta n_{N_{ij}}^{\text{even}} = \frac{i}{2} V_{N_{ij}} \left(\delta n_{N_{ii}}^{\text{even}} - \delta n_{N_{jj}}^{\text{even}} \right) + \text{Re}[F^* F^T]_{ij} G, \quad (3.10b)$$

where Ω_{ij} and G are defined in Eq. (B.3). Note that these are the analogues to Eqs. (B.2), where now an additional term mixes the off-diagonal and diagonal components through the sterile potential term. To make things simpler we focus on the case for which $z_{\text{osc}} < z_{\text{pot}} \ll z_{\text{eq}}$. This enables us to drop the terms proportional to the potential in Eqs. (3.10) and solve them as in the vanilla case (see Eq. (B.4)). One crucial modification, however, appears in the evolution of the sterile charges, with an additional source term proportional to the potential

$$\frac{dq_{N_i}}{dz} = 2 \cdot \mathbb{A}_{\text{ARS}} + 2V_{N_{ij}} \text{Im}[\delta_{N_{ij}}^{\text{odd}}], \quad (3.11)$$

with \mathbb{A}_{ARS} denoting the right-hand side of Eq. (B.6). As described in App. B the vanilla ARS contribution \mathbb{A}_{ARS} vanishes, so in this scenario in the absence of other sources, no net sterile charges are generated until the SM back reaction becomes relevant. In our case, however, the odd off-diagonal components, through the potential, act as sources for q_{N_i} .

Using the zero-th order solutions in Eq. (B.4) one can solve for the charges obtaining

$$q_{N_i}^{\text{analytical}}(z) = V_{N_{ij}} \text{Im}[F^* F^T]_{ij} G \text{Im} \left[iz^2 {}_2F_2 \left[\left\{ \frac{2}{3}, 1 \right\}; \left\{ \frac{4}{3}, \frac{5}{3} \right\}; -\frac{1}{3} iz^3 \Omega_{ij} \right] \right], \quad (3.12)$$

in terms of the generalized hypergeometric function. This result is crucial as it shows that the sterile potential is able to generate charges already at order $\mathcal{O}(F^2)$. This, in turn, implies that a net baryon asymmetry can be produced at order $\mathcal{O}(F^4)$ in contrast to the $\mathcal{O}(F^6)$ suppression in the vanilla ARS scenario. Essentially, two powers of F are replaced by two powers of the new Yukawa coupling Y . Once $z \sim z_{\text{eq}} \gg z_{\text{osc}}$ the oscillations of the off-diagonal correlations are too fast and they average to zero. So the evolution of the flavour asymmetries

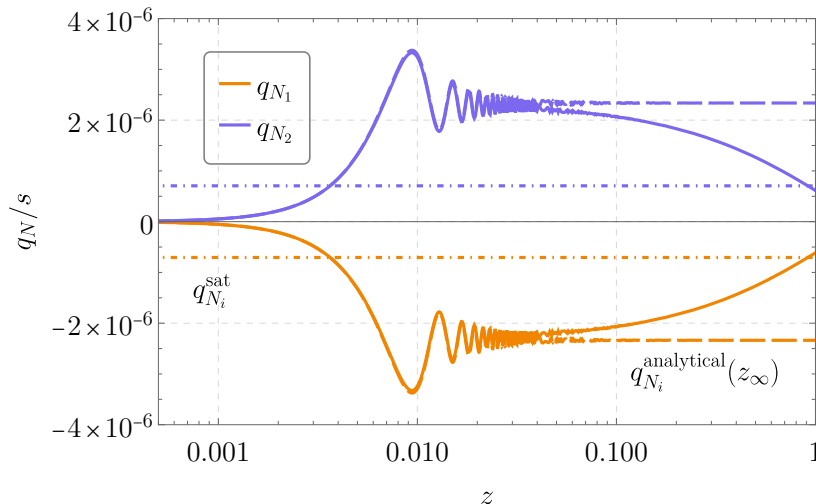


Figure 5: Evolution of the sterile charges with respect to z for the benchmark point. The dashed lines denote the analytical approximations $q_{N_i}^{\text{analytical}}(z)$ discussed in the main text, while the dash-dotted lines indicate the final values $q_{N_i}^{\text{sat}}$.

and the sterile charges at this later stage can be described by

$$\frac{d\Delta_a}{dz} = \frac{\gamma_{AV}}{2} \frac{a_R}{T_{\text{ws}}} \sum_i F_{ia} F_{ai}^\dagger \left(\sum_b (A_{ab} + C_b/2) \Delta_b - q_{N_i} \right) \quad (3.13a)$$

$$\frac{dq_{N_i}}{dz} = -\gamma_{AV} \frac{a_R}{T_{\text{ws}}} \sum_a F_{ia} F_{ai}^\dagger \left(q_{N_i} - \sum_b (A_{ab} + C_b/2) \Delta_b \right) \quad (3.13b)$$

just as in the standard case. Note that Eq. (3.13a) is simply Eq. (2.15) where the source term has been dropped. The solution to this system of equations is formally given by [23]

$$\begin{pmatrix} \Delta_a(z) \\ q_{N_i}(z) \end{pmatrix} = T \exp \left(\gamma_{AV} \frac{a_R}{T_{\text{ws}}} K_{\text{diag}} z \right) T^{-1} \begin{pmatrix} \Delta_a^{\text{osc}}(z_{in}) \\ q_{N_i}^{\text{analytical}}(z_{in}) \end{pmatrix}; \quad (3.14)$$

where $z_{in} \gg z_{\text{osc}}$, so that $q_{N_i}^{\text{analytical}}(z_{in})$ and $\Delta_a^{\text{osc}}(z_{in})$ can be evaluated from Eqs.(3.12) and (B.7) taking the limit $z_{in} \rightarrow \infty$. The matrices K_{diag} and T contain the eigenvalues and eigenvectors of a 5×5 matrix given by

$$K = \begin{pmatrix} \frac{1}{2} \sum_{k=1}^2 F_{ak}^\dagger F_{ka} (A_{ab} + \frac{1}{2}) & -\frac{1}{2} F_{aj}^\dagger F_{ja} \\ \sum_{d=1}^3 F_{id} F_{di}^\dagger (A_{db} + \frac{1}{2} C_b) & -\sum_{d=1}^3 F_{id} F_{di}^\dagger \delta_{ij} \end{pmatrix} \quad (3.15)$$

and $K_{\text{diag}} = T^{-1} K T$. Finally, the baryon asymmetry is given by a simple linear combination

$$B = \frac{28}{79} [\Delta_1(1) + \Delta_2(1) + \Delta_3(1)]. \quad (3.16)$$

This analytical approximation is shown as dashed lines in Fig. 2. To illustrate the generation of the sterile charges, Fig. 5 shows the evolution of q_{N_i} with respect to z for the benchmark point discussed in the last section. The solid lines represent the full numerical solutions, while

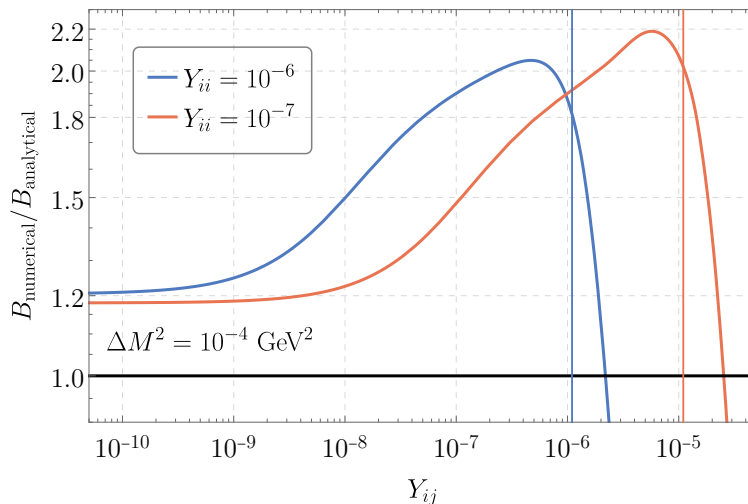


Figure 6: Evolution of the ratio of the full numerical solution and the analytical approximation with respect to the off-diagonal Yukawa elements for different values of the diagonal elements $Y_{ii} = 10^{-6}$ (blue) and $Y_{ii} = 10^{-7}$ (orange) for a fixed mass splitting $\Delta M^2 = 10^{-4} \text{ GeV}^2$. The vertical lines indicate the point at which we expect the analytical approximation to break down.

the dashed lines correspond to the analytical solutions given in Eq. (3.12). We observe that the analytical approximation accurately matches the numerical results up to $z \approx 5 \times 10^{-2}$, beyond which the SM back reaction becomes important and the charges decay. The decay is well approximated by the solution in Eq. (3.14) where we have used $z_{in} \rightarrow \infty$ such that the initial conditions Δ_a^{osc} and $q_{N_i}^{\text{analytical}}$ saturate at a constant value. The solutions to Eq. (3.14) evaluated at $z = 1$ are shown as dash-dotted lines and labeled as $q_{N_i}^{\text{sat}}$ in Fig. 5.

As shown in Fig. 2, however, Equation (3.14) does not fully capture the system's behavior across the entire parameter space. As discussed earlier in this section, neglecting the effects of the new physics rate is only valid for Yukawa couplings $Y_{ij} \lesssim 2 \times 10^{-6}$ when $Y_{ii} = 10^{-6}$. Moreover, our approximation only holds for $z_{\text{osc}} < z_{\text{pot}}$ which leads to the condition

$$Y_{ij} \leq \left(\frac{216\zeta(3)}{\pi a_R} \right)^{2/3} \frac{(\Delta M^2)^{1/3}}{Y_{ii}} \approx 2.4 \times 10^{-11} \frac{(\Delta M^2)^{1/3}}{Y_{ii}}. \quad (3.17)$$

We set the equality and represent this value as vertical lines in Fig. 2. We expect our approximation to break down for larger values of Y_{ij} . To better visualize the performance of Eq. (3.14), Figure 6 finally shows the evolution of the ratio between the full numerical and the analytical solutions as a function of the off-diagonal Y_{ij} . We show two fixed values of $Y_{ii} = 10^{-6}$ (blue) and $Y_{ii} = 10^{-7}$ (orange) for $\Delta M^2 = 10^{-4} \text{ GeV}^2$. The vertical solid lines correspond to the upper value of Y_{ij} for which our approximation breaks down as indicated by the condition in Eq. (3.17). We see that our analytical result differs from the full numerical result by about a factor $\lesssim 2$ in the regime of validity and quickly deteriorates outside of it.

4 Conclusions

Sterile neutrinos are a very simple and compelling extension of the SM, with the potential to address several major open questions in theoretical physics. They could, for instance, explain the origin of neutrino masses, serve as candidates for dark matter, and account for the baryon asymmetry of the Universe. When the masses of the RHNs are below the electroweak scale, leptogenesis can proceed through the ARS mechanism. In this scenario, the baryon asymmetry is generated via the CP-violating oscillations of the sterile neutrinos. At the same time, the sterile neutrinos remain out of equilibrium with the SM until after electroweak symmetry breaking and act as reservoir that hides a fraction of the lepton number from the sphalerons. However, in order to generate the observed BAU, the oscillation timescale, which is set by the mass difference between the sterile neutrinos, cannot be too short compared to the time of sphaleron freeze-out. This necessitates a high degree of degeneracy between the masses, such that GeV sterile neutrinos end up needing to have mass differences of just a few tens of keV. In this work, we show that adding self-interactions among the RHNs can significantly alleviate this fine-tuned mass condition. To explore this, we employ a scalar-mediated interaction with Yukawa-like couplings to the sterile neutrinos. The new interaction has two main effects on the system: 1) it introduces corrections to the neutrino's self-energy and 2) it opens new creation and destruction channels for the sterile neutrinos. This leads to two new time scales that can have an impact on the dynamics. We find that, within the oscillatory regime, the system is dominated by the effects of the thermal potential over a significant portion of the parameter space. In this limit, we can solve the quantum kinetic equations analytically and provide an approximation for the BAU. It agrees with the full numerical solution within a factor of two in its range of validity. Interestingly, we find that the baryon asymmetry can be enhanced by several orders of magnitude due to the new interactions. This relaxes the mass splitting constraint of the vanilla ARS significantly and allows to generate the observed BAU without a strong tuning of the masses.

Our results show promising new directions to study within the ARS mechanism and more research is needed to explore the possibilities further. In full generality, this is a complicated problem since the different time scales in the problem can arrange in various ways and already within the vanilla ARS mechanism other regimes with alternative solutions are known to exist, see e.g. the discussion of the strongly overdamped regime in [23]. We have not attempted to explore these alternative regions of the parameter space systematically and it remains an interesting question what effects the new self-interactions can have there. In addition, we have applied some simplifications to the system to reduce the number of degrees of freedom. For instance, this paper focuses on the case in which the diagonal elements of the Yukawa matrix are equal. Exploring the more general case with $Y_{ii} \neq Y_{jj}$ remains a task for future work. Finally, a comprehensive phenomenological study would be highly desirable to connect the effects of particle dynamics in the early Universe with observables that can be tested in the laboratory today, e.g. direct and indirect searches for heavy sterile neutrinos (see [34] for a summary) or searches for new light scalars at the LHC.

A The Casas-Ibarra parametrization

For the system considered in this work, the Yukawa matrix F appearing in Eq. (2.1) can be written using the Casas-Ibarra parametrization [32]

$$F^\dagger = \frac{1}{v} U_\nu \sqrt{m^{\text{diag}}} \mathcal{R} \sqrt{M^{\text{diag}}}, \quad (\text{A.1})$$

where $v = 246$ GeV is the vacuum expectation value of the Higgs and the diagonal matrices m and M contain the masses for the active and the sterile neutrinos, respectively. In the same way U_ν is the PMNS matrix that we parametrize as

$$U_\nu = \begin{pmatrix} c_{12}c_{13} & c_{13}s_{12} & s_{13}e^{-i\delta} \\ -c_{23}s_{12} - c_{12}e^{i\delta} & c_{12}c_{23} - s_{12}s_{13}s_{23}e^{i\delta} & c_{13}s_{23} \\ -c_{12}c_{23}s_{13}e^{i\delta} + s_{12}s_{23} & -c_{23}s_{12}s_{13}e^{i\delta} - c_{12}s_{23} & c_{13}c_{23} \end{pmatrix} \cdot \begin{pmatrix} e^{\frac{i}{2}\alpha_1} & 0 & 0 \\ 0 & 1 & 0 \\ 0 & 0 & e^{\frac{i}{2}\alpha_2} \end{pmatrix}, \quad (\text{A.2})$$

where for readability we have used the notation $s_{ij} = \sin(\theta_{ij})$ and $c_{ij} = \cos(\theta_{ij})$. In this parametrization, θ_{ij} are the so-called mixing angles, while δ is a Dirac phase and $\alpha_{i,j}$ are Majorana phases. In analogy with the PMNS matrix for the active sector, the matrix \mathcal{R} measures the misalignment between the mass and the interaction eigenstates of the sterile neutrinos. For two sterile neutrinos and normal hierarchy, it takes the form

$$\mathcal{R} = \begin{pmatrix} 0 & 0 \\ \cos(\omega) & \sin(\omega) \\ -\sin(\omega) & \cos(\omega) \end{pmatrix}, \quad (\text{A.3})$$

with ω a complex angle so that \mathcal{R} is orthogonal. Not all input parameters are on the same footing here. On the one hand, the mixing angles for the PMNS matrix are well determined by observations and its CP phases are at least mildly constrained. On the other hand, ω is currently completely undetermined. It parametrizes our ignorance of the details of the Yukawa couplings of the sterile neutrinos.

B Analytical approach to standard ARS

In this appendix we review the analytical solution for the ARS scenario in the oscillatory regime. Analytical solutions in this regime have been put forward in, e.g. Refs. [6, 24, 35, 36]. Here, we focus on the solution of Ref. [23] and we refer the reader to this reference for more details.

Let us start by considering the system at early times, for $z \sim z_{\text{osc}}$. The condition $z_{\text{osc}} \ll z_{\text{eq}}$ allows us to simplify Eq. (2.11) in two ways. First, we can neglect the backreaction term from the SM driven by $\tilde{\Gamma}$, since it only becomes important at later times for $z \gg z_{\text{osc}}$. Thus Eq. (2.11) reduces to ⁵

$$\frac{d}{dz} \delta n_{N^\pm} + \frac{i}{2} z^2 [H_{N^\pm}^{\text{vac}}, \delta n_{N^\pm}] = -\frac{1}{2} \{\Gamma_{N^\pm}, \delta n_{N^\pm}\}. \quad (\text{B.1})$$

Note that, in the following, we only focus on the equations for $\delta n_{N_{ij}}^{\text{odd/even}}$ and $\delta n_{N_{ii}}^{\text{odd}}$ since the diagonal even components are not relevant for the generation of the BAU. Secondly, we can perform an iterative solution for small $|F^* F^T|$. In this way, the first non-vanishing contributions can be obtained by replacing $(\delta n_{N^\pm})_{ij} \rightarrow -n_{\text{eq}} \delta_{ij}$ on the right-hand side of

⁵Given that $H_{N^\pm}^{\text{th}}$ is generated by forward scattering of neutrinos through the F couplings, it is diagonal in the flavour basis. This means that, at early times, $H_{N^\pm}^{\text{th}}$ commutes with δn_{N^\pm} and therefore we neglected its contribution in Eq. (B.1).

Eq. (2.11). With these simplifications we are left with two equations for the off-diagonal components

$$\begin{aligned}\frac{d}{dz}\delta n_{N_{ij}}^{\text{odd}} + i\Omega_{ij}z^2\delta n_{N_{ij}}^{\text{odd}} &= -i\text{Im}[F^*F^T]_{ij}G, \\ \frac{d}{dz}\delta n_{N_{ij}}^{\text{even}} + i\Omega_{ij}z^2\delta n_{N_{ij}}^{\text{even}} &= \text{Re}[F^*F^T]_{ij}G,\end{aligned}\tag{B.2}$$

where

$$\Omega_{ij} = \frac{a_R\pi^2}{T_{\text{ws}}^3 36\zeta(3)} (M_{ii}^2 - M_{jj}^2), \quad \text{and} \quad G = \gamma_{AV} \frac{a_R n_{\text{eq}}}{T_{\text{ws}}}.\tag{B.3}$$

The solutions to Eqs. (B.2) are given by

$$\delta n_{N_{ij}}^{\text{odd}} = -i\text{Im}[F^*F^T]_{ij}G\mathcal{F}_{ij}, \quad \text{and} \quad \delta n_{N_{ij}}^{\text{even}} = \text{Re}[F^*F^T]_{ij}G\mathcal{F}_{ij},\tag{B.4}$$

in terms of the function \mathcal{F}_{ij} which is defined as

$$\mathcal{F}_{ij} = \exp\left(-\frac{1}{3}i\Omega_{ij}z^3\right) \left[\frac{\Gamma\left(\frac{1}{3}\right) - \Gamma\left(\frac{1}{3}, -\frac{1}{3}i\Omega_{ij}z^3\right)}{3^{2/3}(-i\Omega_{ij})^{1/3}} \right].\tag{B.5}$$

Similarly, the evolution of sterile charges, given by the odd diagonal components, is described by

$$\begin{aligned}\frac{d}{dz}\delta n_{N_{ii}}^{\text{odd}} &= -\gamma_{AV} \frac{a_R}{T_{\text{ws}}} \left[\text{Re}[F^*F^T]_{ii}\delta n_{N_{ii}}^{\text{odd}} + \right. \\ &\quad \left. \sum_{\substack{j \\ j \neq i}} \left(\text{Re}[F^*F^T]_{ij}\text{Re}[\delta n_{N_{ij}}^{\text{odd}}] + \text{Im}[F^*F^T]_{ij}\text{Im}[\delta n_{N_{ij}}^{\text{even}}] \right) \right].\end{aligned}\tag{B.6}$$

It follows from Eq. (B.4) that the source term in Eq. (B.6) vanishes and no sterile charges are generated at this level. Consequently, in the standard ARS mechanism, a net baryon asymmetry is established only at later times, at order $\mathcal{O}(F^6)$, due to the washout effects from the SM. Nonetheless, flavour asymmetries of order $\mathcal{O}(F^4)$ are produced already at z_{osc} through the source term in Eq. (2.16)

$$\Delta_a^{\text{osc}}(z) = -\int_0^z \frac{dz'}{T_{\text{ws}}} S_a,\tag{B.7}$$

which, at this stage, satisfy $\sum_{a=e,\mu,\tau} \Delta_a = 0$.

Once $z \sim z_{\text{eq}} \gg z_{\text{osc}}$ the oscillations of the off-diagonal correlations (B.4) are too fast and they average to zero. So the evolution of the flavour asymmetries and the sterile charges at this later stage can be described by Eqs. (3.13). The solution is then given by Eq. (3.14), where now we take as initial conditions $q_{N_i}(z_{in}) = 0$ and

$$\Delta_a^{\text{osc}}(z_{in}) = -\frac{iz^2}{2T_{\text{ws}}} a_R \gamma_{AV} G \left(\sum_{\substack{i,j,c \\ i \neq j}} F_{ai}^\dagger F_{ic} F_{cj}^\dagger F_{ja} \text{Im} \left[{}_2F_2 \left[\left\{ \frac{2}{3}, 1 \right\}; \left\{ \frac{4}{3}, \frac{5}{3} \right\}; -\frac{1}{3}iz^3\Omega_{ij} \right] \right] \right) \Bigg|_{z \rightarrow \infty},\tag{B.8}$$

which is the analytical solution to Eq.(B.7).

Acknowledgments

MD and SV acknowledge support by the DFG via the the individual research grant Nr. 496940663.

References

- [1] **Planck** Collaboration, N. Aghanim et al., *Planck 2018 results. VI. Cosmological parameters*, *Astron. Astrophys.* **641** (2020) A6, [[arXiv:1807.06209](#)]. [Erratum: *Astron. Astrophys.* 652, C4 (2021)].
- [2] **Particle Data Group** Collaboration, S. Navas et al., *Review of particle physics*, *Phys. Rev. D* **110** (2024), no. 3 030001.
- [3] T.-H. Yeh, J. Shelton, K. A. Olive, and B. D. Fields, *Probing physics beyond the standard model: limits from BBN and the CMB independently and combined*, *JCAP* **10** (2022) 046, [[arXiv:2207.13133](#)].
- [4] M. Fukugita and T. Yanagida, *Baryogenesis Without Grand Unification*, *Phys. Lett. B* **174** (1986) 45–47.
- [5] V. A. Kuzmin, V. A. Rubakov, and M. E. Shaposhnikov, *On the Anomalous Electroweak Baryon Number Nonconservation in the Early Universe*, *Phys. Lett. B* **155** (1985) 36.
- [6] T. Asaka and M. Shaposhnikov, *The ν MSM, dark matter and baryon asymmetry of the universe*, *Phys. Lett. B* **620** (2005) 17–26, [[hep-ph/0505013](#)].
- [7] T. Asaka, S. Blanchet, and M. Shaposhnikov, *The ν MSM, dark matter and neutrino masses*, *Phys. Lett. B* **631** (2005) 151–156, [[hep-ph/0503065](#)].
- [8] M. Shaposhnikov, *The ν MSM, leptonic asymmetries, and properties of singlet fermions*, *JHEP* **08** (2008) 008, [[arXiv:0804.4542](#)].
- [9] T. Asaka and H. Ishida, *Flavour Mixing of Neutrinos and Baryon Asymmetry of the Universe*, *Phys. Lett. B* **692** (2010) 105–113, [[arXiv:1004.5491](#)].
- [10] L. Canetti and M. Shaposhnikov, *Baryon Asymmetry of the Universe in the ν MSM*, *JCAP* **09** (2010) 001, [[arXiv:1006.0133](#)].
- [11] A. Pilaftsis, *CP violation and baryogenesis due to heavy Majorana neutrinos*, *Phys. Rev. D* **56** (1997) 5431–5451, [[hep-ph/9707235](#)].
- [12] A. Pilaftsis and T. E. J. Underwood, *Resonant leptogenesis*, *Nucl. Phys. B* **692** (2004) 303–345, [[hep-ph/0309342](#)].
- [13] E. K. Akhmedov, V. A. Rubakov, and A. Y. Smirnov, *Baryogenesis via neutrino oscillations*, *Phys. Rev. Lett.* **81** (1998) 1359–1362, [[hep-ph/9803255](#)].
- [14] M. Drewes, B. Garbrecht, P. Hernandez, M. Kekic, J. Lopez-Pavon, J. Racker, N. Rius, J. Salvado, and D. Teresi, *ARS Leptogenesis*, *Int. J. Mod. Phys. A* **33** (2018), no. 05n06 1842002, [[arXiv:1711.02862](#)].
- [15] J. Beacham et al., *Physics Beyond Colliders at CERN: Beyond the Standard Model Working Group Report*, *J. Phys. G* **47** (2020), no. 1 010501, [[arXiv:1901.09966](#)].
- [16] I. Flood, R. Porto, J. Schlesinger, B. Shuve, and M. Thum, *Hidden-sector neutrinos and freeze-in leptogenesis*, *Phys. Rev. D* **105** (2022), no. 9 095025, [[arXiv:2109.10908](#)].
- [17] O. Fischer, M. Lindner, and S. van der Woude, *Robustness of ARS leptogenesis in scalar extensions*, *JHEP* **05** (2022) 149, [[arXiv:2110.14499](#)].
- [18] M. Escudero and S. J. Witte, *The hubble tension as a hint of leptogenesis and neutrino mass generation*, *Eur. Phys. J. C* **81** (2021), no. 6 515, [[arXiv:2103.03249](#)].

- [19] A. Caputo, P. Hernandez, and N. Rius, *Leptogenesis from oscillations and dark matter*, *Eur. Phys. J. C* **79** (2019), no. 7 574, [[arXiv:1807.03309](#)].
- [20] T. Alanne, T. Hügler, M. Platscher, and K. Schmitz, *Low-scale leptogenesis assisted by a real scalar singlet*, *JCAP* **03** (2019) 037, [[arXiv:1812.04421](#)].
- [21] A. D. Sakharov, *Violation of CP Invariance, C asymmetry, and baryon asymmetry of the universe*, *Pisma Zh. Eksp. Teor. Fiz.* **5** (1967) 32–35.
- [22] T. Hambye and D. Teresi, *Baryogenesis from L-violating Higgs-doublet decay in the density-matrix formalism*, *Phys. Rev. D* **96** (2017), no. 1 015031, [[arXiv:1705.00016](#)].
- [23] M. Drewes, B. Garbrecht, D. Gueter, and J. Klaric, *Leptogenesis from Oscillations of Heavy Neutrinos with Large Mixing Angles*, *JHEP* **12** (2016) 150, [[arXiv:1606.06690](#)].
- [24] M. Drewes and B. Garbrecht, *Leptogenesis from a GeV Seesaw without Mass Degeneracy*, *JHEP* **03** (2013) 096, [[arXiv:1206.5537](#)].
- [25] A. D. Dolgov, *Neutrinos in the Early Universe*, *Sov. J. Nucl. Phys.* **33** (1981) 700–706.
- [26] G. Sigl and G. Raffelt, *General kinetic description of relativistic mixed neutrinos*, *Nucl. Phys. B* **406** (1993) 423–451.
- [27] R. Barbieri and A. Dolgov, *Neutrino oscillations in the early universe*, *Nucl. Phys. B* **349** (1991) 743–753.
- [28] T. Asaka, S. Eijima, and H. Ishida, *Kinetic Equations for Baryogenesis via Sterile Neutrino Oscillation*, *JCAP* **02** (2012) 021, [[arXiv:1112.5565](#)].
- [29] D. Notzold and G. Raffelt, *Neutrino Dispersion at Finite Temperature and Density*, *Nucl. Phys. B* **307** (1988) 924–936.
- [30] C. Quimbay and S. Vargas-Castrillon, *Fermionic dispersion relations in the standard model at finite temperature*, *Nucl. Phys. B* **451** (1995) 265–304, [[hep-ph/9504410](#)].
- [31] M. D. Astros and S. Vogl, *Boosting the production of sterile neutrino dark matter with self-interactions*, *JHEP* **03** (2024) 032, [[arXiv:2307.15565](#)].
- [32] J. A. Casas and A. Ibarra, *Oscillating neutrinos and $\mu \rightarrow e, \gamma$* , *Nucl. Phys. B* **618** (2001) 171–204, [[hep-ph/0103065](#)].
- [33] M. C. Gonzalez-Garcia, M. Maltoni, and T. Schwetz, *NuFIT: Three-Flavour Global Analyses of Neutrino Oscillation Experiments*, *Universe* **7** (2021), no. 12 459, [[arXiv:2111.03086](#)].
- [34] M. Drewes and B. Garbrecht, *Combining experimental and cosmological constraints on heavy neutrinos*, *Nucl. Phys. B* **921** (2017) 250–315, [[arXiv:1502.00477](#)].
- [35] A. Abada, G. Arcadi, V. Domcke, and M. Lucente, *Lepton number violation as a key to low-scale leptogenesis*, *JCAP* **11** (2015) 041, [[arXiv:1507.06215](#)].
- [36] P. Hernández, M. Kekic, J. López-Pavón, J. Racker, and N. Rius, *Leptogenesis in GeV scale seesaw models*, *JHEP* **10** (2015) 067, [[arXiv:1508.03676](#)].